Monthly Notices of the ROYAL ASTRONOMICAL SOCIETY

MNRAS **450,** 4292–4300 (2015) doi:10.1093/mnras/stv720

VLT spectroscopy of the black hole candidate Swift J1357.2−0933 in quiescence

M. A. P. Torres,[1,2,3★] P. G. Jonker,[1,2] J. C. A. Miller-Jones,[4] D. Steeghs,[5] S. Repetto[2] and Jianfeng Wu[6]

[1]*SRON, Netherlands Institute for Space Research, Sorbonnelaan 2, NL-3584 CA Utrecht, the Netherlands*
[2]*Department of Astrophysics/ IMAPP, Radboud University Nijmegen, Heyendaalseweg 135, NL-6525 AJ Nijmegen, the Netherlands*
[3]*European Southern Observatory. Alonso de Córdova 3107, Vitacura, Casilla 19001, Santiago de Chile, Chile*
[4]*International Centre for Radio Astronomy Research, Curtin University, GPO Box U1987, Perth, WA 6845, Australia*
[5]*Department of Physics, University of Warwick, Coventry CV4 7AL, UK*
[6]*Harvard–Smithsonian Center for Astrophysics, 60 Garden Street, Cambridge, MA 02138, USA*

Accepted 2015 March 30. Received 2015 March 8; in original form 2014 August 29

ABSTRACT

We present time-resolved optical spectroscopy of the counterpart to the high-inclination black hole low-mass X-ray binary Swift J1357.2−0933 in quiescence. Absorption features from the mass donor star were not detected. Instead the spectra display prominent broad double-peaked H α emission and weaker He I emission lines. From the H α peak-to-peak separation, we constrain the radial velocity semi-amplitude of the donor star to $K_2 > 789\,\mathrm{km\,s^{-1}}$. Further analysis through radial velocity and equivalent width measurements indicates that the H α line is free of variability due to S-wave components or disc eclipses. From our data and previous observations during outburst, we conclude that long-term radial velocity changes ascribed to a precessing disc were of low amplitude or not present. This implies that the centroid position of the line should closely represent the systemic radial velocity, γ. Using the derived $\gamma = -150$ km s^{-1} and the best available limits on the source distance, we infer that the black hole is moving towards the plane in its current Galactic orbit unless the proper motion is substantial. Finally, the depth of the central absorption in the double-peaked profiles adds support for Swift J1357.2−0933 as a high-inclination system. On the other hand, we argue that the low hydrogen column density inferred from X-ray fitting suggests that the system is not seen edge-on.

Key words: accretion, accretion discs – black hole physics – binaries: close – stars: individual: Swift J1357.2−0933 – X–rays: binaries.

1 INTRODUCTION

The X-ray transient Swift J1357.2−0933 (hereafter J1357.2) was discovered in outburst on 2011 January 28 with the Burst Alert Telescope on board *Swift* (Krimm et al. 2011a). Follow-up observations with the *Swift* X-ray Telescope revealed a spectrum consistent with an absorbed power law with a low hydrogen column density $N_{\rm H}$ of $(1.2 \pm 0.7) \times 10^{20}$ cm^{-2} and a photon index that evolved from $\Gamma = 1.5$ to 2.1 during the outburst decline (Krimm, Kennea & Holland 2011b; Armas-Padilla et al. 2013). A 0.5−10 keV outburst peak luminosity of $1.1 \times 10^{35} \times (\frac{d}{1.5\,\mathrm{kpc}})^2$ erg s^{-1} is inferred from these observations. In addition, *XMM*–Newton data obtained on 2011 February 5 could be fitted with a three-component model: the above mentioned power law with a 93 per cent contribution to the total flux, a thermal (disc) component with $kT = 0.2$ keV and one edge at 0.73 keV (Armas-Padilla et al. 2014a). The thermal component is interpreted as soft emission originating in the accretion disc, while the edge is associated with interstellar iron. The low X-ray peak luminosity together with the evolution (softening) of the power-law dominated spectrum, the low temperature for the thermal component associated with the accretion disc and the detection of radio emission (Sivakoff, Miller-Jones & Krimm 2011) are in accordance with the source being a black hole system in the low-hard state through the entire outburst. In this regard, timing analysis of both the *XMM*–Newton data as well as contemporaneous *RXTE* Proportional Counter Array observations showed a power spectrum with characteristics more similar to those detected in the low-hard state of black holes than neutron stars (Armas-Padilla et al. 2014a). On the other hand, early in the outburst a 6 mHz-quasi-periodic oscillation was detected in one of the *RXTE* observations. This low frequency is atypical in black holes and more common in dipping neutron stars (see Armas-Padilla et al. 2014a for details).

J1357.2 was observed in quiescence with *XMM*–Newton on 2013 July 10 and detected at a 0.5–10 keV X-ray luminosity of

★ E-mail: M.Torres@sron.nl

$8.5^{+5.5}_{-2.6} \times 10^{29} \times (\frac{d}{1.5\mathrm{kpc}})^2$ erg s^{-1} (Armas-Padilla et al. 2014b). The X-ray spectrum in quiescence is consistent with an absorbed power law with $\Gamma = 2.1 \pm 0.4$, although fits to single thermal models were also permitted by the data.

The optical and near-infrared counterparts to J1357.2 were identified with a $r' \simeq 16.30$ and $K = 17.4$ mag star[1] (Rau et al. 2011). A high-resolution optical spectrum obtained on 2011 February 2 showed no clear indication for emission lines, lack of diffuse interstellar bands and the presence of weak absorption lines from the interstellar Na doublet (Torres et al. 2011). A low-resolution spectrum taken one day later exhibited weak and broad Hα and Hβ emission lines with the former having 7 Å equivalent width (EW) and ∼4000 km s^{-1} full width at zero intensity (FWZI; Milisavljevic et al. 2011). High-resolution Hα spectroscopy undertaken on 2011 February 25–27 resolved the very broad double-peaked line profile with a peak-to-peak separation of ∼1800 km s^{-1} (Casares et al. 2011). Further time-resolved observations allowed Corral-Santana et al. (2013) to find a 2.8 ± 0.3 h modulation in radial velocities extracted from the Hα line profile. Assuming this periodicity corresponds to the orbital period and using the line peak-to-peak separation to constrain the radial velocity semi-amplitude of the donor star to $K_2 \geq 690$ km s^{-1}, a mass larger than 3.0 M$_\odot$ is estimated for the compact object. Complementary time-resolved optical photometry did not show any evidence for variability with the above periodicity (Corral-Santana et al. 2013). The light curves show dipping variability with a recurrence time that gradually increases from 2.3 to 7.5 min over 69 d of follow-up photometry. The recurrent optical dips (up to 0.8 mag) are interpreted as obscuration events caused by a toroidal structure with asymmetric height with respect to the orbital plane. In this scenario, the changes in the dipping frequency would imply that this structure is moving inside-out the disc during outburst. In order to produce the profound dips in the light curve, a very large system inclination is necessary. However, neither the optical data nor the X-ray data showed dips or eclipses due to the donor star (Armas-Padilla et al. 2013; Corral-Santana et al. 2013). To explain the non-detection of these features in the light curve, Corral-Santana et al. (2013) invoke an accreting binary configuration in which the mass ratio is low enough to have a Roche lobe filling donor star with a radius smaller or similar to the disc outer rim.

The optical counterpart to J1357.2 was also identified in quiescence at r=21.96 in Sloan Digital Sky Survey (SDSS) images taken in 2006 May (Rau et al. 2011). Based on the SDSS pre-outburst colours and assuming no disc contribution to the optical light, the donor star was tentatively classified as an M4 dwarf at ∼1.5 kpc distance. This is in good agreement with the M4.5 donor at ∼1.6 kpc expected from a Roche lobe filling donor in a 2.8-h-orbital period system (Corral-Santana et al. 2013). However, time-resolved photometry during quiescence at different post-outburst epochs (Shahbaz et al. 2013) reveals a very different picture: the donor star is not the dominant source of light at optical or infrared wavelengths. The multicolour light curves lack evidence of any orbital variability caused by the donor star, i.e. ellipsoidal modulations, eclipses or dip features. Instead the photometry shows flares of up to ∼1.5 and ∼2 mag at optical and infrared wavelengths, respectively. This is the largest flare amplitude known in quiescent black hole X-ray binaries. Moreover, the dipping behaviour observed in outburst persists in quiescence but with a ∼30 min recurrence time. Both the optical to mid-infrared quiescent spectral energy distribution (SED) and optical variability SED of J1357.2 can be described by a single power-law model with index $\Gamma \sim 1.4$. This steep power law together with the high-amplitude flickering is interpreted as due to synchrotron emission from a variable, weak jet that dominates the SED over the donor star light (Shahbaz et al. 2013). Using the relation between orbital period and the outburst optical amplitude, Shahbaz et al. constrain the distance towards J1357.2 to be between 0.5 and 6.3 kpc.

The lack of accurate dynamical parameters and observational details of the accretion disc structure during quiescence motivated us to perform time-resolved optical spectroscopy. We begin with a description of the observations and data reduction steps (Section 2). The average optical spectrum of J1357.2 in quiescence is presented in Section 3 where we also characterize the Hα line profile and constrain its variability. Finally, the results are presented and discussed in Section 4, where we examine key questions such as the orbital parameters and space velocity for the system. Our conclusions are summarized in Section 5.

2 OBSERVATIONS AND DATA REDUCTION

Time-resolved optical spectroscopy of J1357.2 was obtained with the FOcal Reducer and low dispersion Spectrograph 2 (FORS2, Appenzeller et al. 1998) which is mounted on the Cassegrain focus of the 8.2-m ESO Unit 1 Very Large Telescope at Paranal, Chile. The observations were obtained in service mode under programme 091.D-0865(A) during 2013 April 14 5:37 – 6:22 UT, 2013 April 18 4:35 – 8:00 UT and 2013 May 4 4:12 – 4:57 UT. FORS2 was used with the standard resolution collimator and the 2048 × 4096 pixels MIT two CCDs mosaic detector binned 2 × 2 to provide a 0.25 arcsec pixel^{-1} scale. The instrument was operated in long-slit mode with the 600 line mm^{-1} grism GRIS_600RI. J1357.2 was centred in a 1.0 arcsec wide slit with its location offset from the CCD centre. This instrumental setup yields a dispersion of 1.6 Å pixel^{-1}, a coverage in the spectral range λλ5300–8630 and a slitwidth-limited resolution of ∼5 Å full-width half-maximum (FWHM). A total of six 1 h-long observing blocks (OBs) were executed consisting of four spectroscopic integrations of 640 s each. Four, sixteen and four spectra were collected on April 14 at sec $z < 1.08$, April 18 from sec z 1.04 to 1.43 and May 4 at sec $z < 1.07$, respectively. We measure from the width of the source spatial profile at spectral positions covering Hα an image quality between 0.6–0.8 , 0.5–0.7 and 0.7 − 0.8 arcsec for the first, second and third nights, respectively and a mean 0.66 ± 0.07 arcsec FWHM from the three nights. Therefore, the observations were obtained in seeing-limited conditions yielding a spectral resolution of ∼3 Å FWHM corresponding to 140 km s^{-1} at Hα.

The spectra were reduced and extracted using standard techniques implemented in the STARLINK, FIGARO and PAMELA packages while the wavelength calibration was done with MOLLY. The data reduction consisted of debiasing and flat-fielding the data. The spectra were extracted using the algorithm of Horne (1986) to optimize the signal-to-noise ratio of the resulting spectra. Exposures using comparison arc lamps were performed after the end of each night in order to establish the pixel-to-wavelength scale. This was derived through polynomial fits to 27 arc lines. The rms scatter of the fit was always <0.07 Å, which is less than 1/22 of the wavelength dispersion. The sky [O I] λλ5577.34, 6300.3 lines and the OH emission blend at 7316.3 Å showed that wavelength zero-point disparities reached up to $\lesssim$30 km s^{-1} in amplitude. These deviations were corrected for by

[1] The coordinates in Rau, Greiner & Filgas (2011) are incorrect due to a typographical error. The coordinates for J1357.2 are $\alpha(J2000) = 13{:}57{:}16.829$ and $\delta(J2000) = -09{:}32{:}38.75$ as provided by SDSS (Abazajian et al. 2009).

applying to the spectra zero-point shifts calculated using the [O I] λ6300.3 emission feature. The resulting 24 spectra were normalized by dividing each of them by a low-order spline fit to the continuum after masking out emission lines and atmospheric absorption bands. Finally, the resulting spectra were rebinned to a uniform pixel scale.

Since all the observations were seeing limited, systematic effects due to excursions of the target position with respect to the slit centre may affect the radial velocity determinations presented in this work. In this regard, J1357.2 was centred on the slit at the start of each OB execution, except perhaps during the last two OBs on April 18. For these OBs, we lack the reacquisition and through-slit images commonly saved when the centring is checked or performed during service mode observations. In what follows we will conservatively assume that for both OBs the centring step was skipped. Hence, positional departures from the exact slit centre and changes in the target position during the spectroscopic exposures have certainly happened. Unfortunately, we lack the data required to quantify and correct for this effect (see e. g. Bassa et al. 2006). Section 2.4.3 in the ESO FORS2 manual (Issue 92.0) offers constraints on the image motion for a given z due to instrument flexures. This motion increases with z. As our observations were performed after culmination, z increased monotonously and it is therefore reasonable to assume that the offsets in the target position accumulate. Thus, we estimate a cumulative offset <0.3 (binned) pixels at the end of the execution of the single OBs during April 14 and May 4 . The cumulative offsets at the end of the four OBs executed on April 18 are estimated to be <0.3, <0.3, <0.7, <1.1 binned pixels. The systematic effects could therefore have introduced radial velocity offsets (at Hα) from <22 to <84 km s^{-1}. We have measured the positional offsets along the spatial direction. For this, we have calculated the centroid for the spatial profile of J1357.2 at Hα in all spectra. The centroids differ by <0.3 (binned) pixels. This suggests that the cumulative positional offsets in the dispersion direction during April 18 may be smaller than estimated if they have a similar amplitude to that measured for the offsets in the spatial direction.

3 DATA ANALYSIS

3.1 Averaged spectral features

In Fig. 1, we present the result obtained by averaging the 24 individual FORS2 spectra. The averaged data show no evidence for photospheric features from the donor star such as the TiO bands characteristic of M-type stars. The interstellar sodium doublet found in outburst by Torres et al. (2011) is not obvious due to the low reddening towards the source and the fact that this feature falls on top of the He I λ5876 emission line. All significant absorption features in the spectrum are caused by the Earth's atmosphere. The spectrum is dominated by a prominent broad and double-peaked Hα emission line together with weaker emission lines of He I λλ5876, 6678, 7065. He I λ5876 is also double peaked while He I λ6678 is partially resolved from the Hα line red wing. At red wavelengths, there is no obvious emission from Paschen lines or the two Ca II triplet components covered by the data. The apparent emission feature at ∼λ8492–3 is not coincident with any of the above hydrogen or Ca II lines and it is most likely an artefact.

The mean Hα and He I λ5876 double-peaked line profiles were fitted with one and two-Gaussian functions using the Marquardt

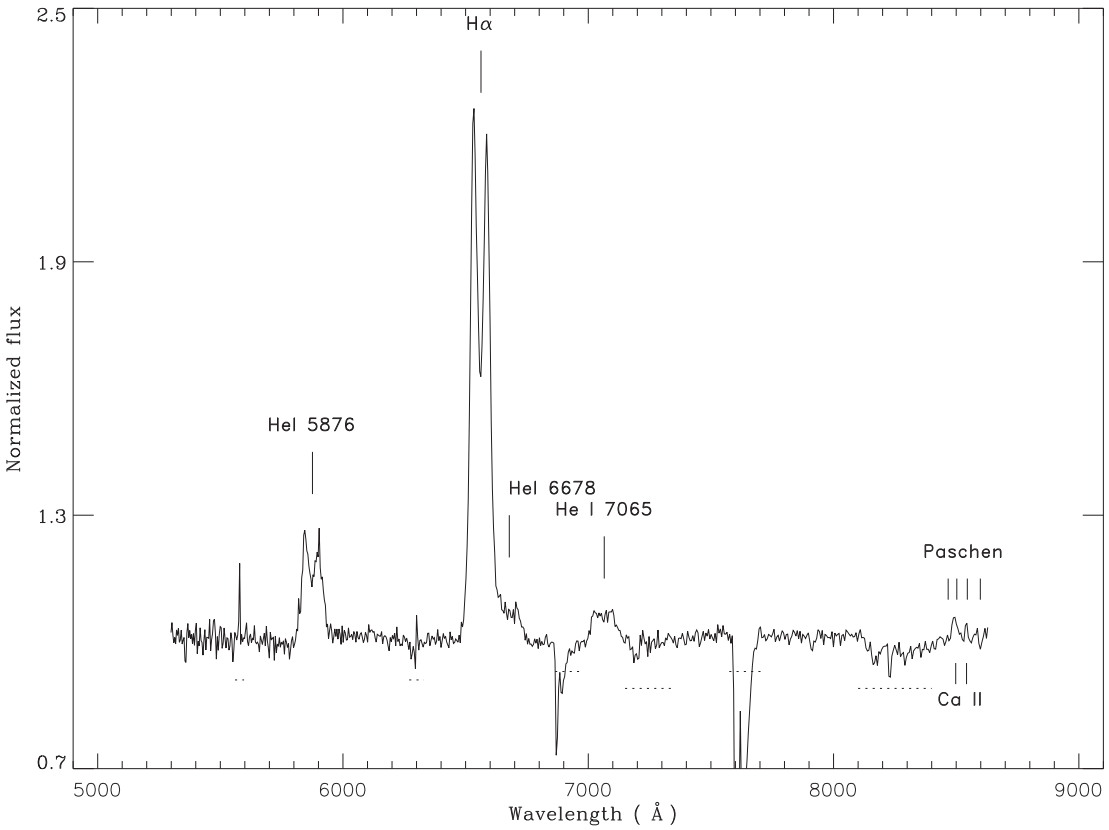

Figure 1. Continuum-normalized and averaged optical spectrum of J1357.2 in quiescence. The rest wavelengths for Hα and identified He I disc lines are provided. For the sake of clarity, we also mark the rest wavelengths for the two Ca II infrared components at λλ8498, 8542 and Paschen lines at λλ8467, 8502, 8545, 8598. The dashed lines below the source continuum mark the location of strong telluric features and residual sky emission lines.

Table 1. Emission line parameters: centroid and peak-to-peak separation (ΔV^{pp}) derived from a two-Gaussian fit to the line profiles (except for He I λ7065 where the line was fitted with a single Gaussian). The FWHM was derived from a single Gaussian fit and corrected for the instrumental spectral resolution. The uncertainties for the centroid, peak-to-peak separation and FWHM were calculated after scaling the data error bars to yield a fit with $\chi^2/\mathrm{d.o.f} = 1$. The uncertainties in the EWs are estimated by determining the scatter in the values derived when selecting different wavelength intervals to set the local continuum level. The FWZIs are given as lower limits since the ability to determinate the extension of the line wings is usually set by the signal to noise in the data.

	H α	He I 5876	He I 7065
Centroid (km s^{-1})	-137 ± 8	-180 ± 40	-100 ± 100
ΔV^{pp} (km s^{-1})	2340 ± 20	2640 ± 70	–
FWHM (km s^{-1})	4025 ± 110	4500 ± 200	4290 ± 250
FWZI (km s^{-1})	$\gtrsim$6300	$\gtrsim$7040	$\gtrsim$5900
EW (Å)	-92 ± 1	-19 ± 1	-9 ± 2

algorithm (Bevington 1969). From the one-Gaussian fit, we derive the line FWHM given in Table 1. The two-Gaussian model allows us to measure the velocity shifts of the blue (V_b) and red (V_r) peaks with respect to the line rest wavelength. Their difference $\Delta V^{pp} = V_r - V_b$ (peak-to-peak separation) and mean $(V_r + V_b)/2$ (centroid of the line) are included in Table 1. This table also lists the measured FWZI and EWs for H α and He I λλ5876, 7065. The mean FWHM for H α is consistent with the ∼3900 km s^{-1} FWHM found for this line in low-resolution spectroscopy obtained on 2013 April 29 UT (Shahbaz et al. 2013), although on that occasion the line profile appeared single peaked and with −120 Å EW. This value is below the maximum EW observed when studying the time variability of H α (Section 3.2).

The mean peak-to-peak velocity separations for the H α and He I λ5876 lines are 2340 ± 20 and 2640 ± 70 km s^{-1}, respectively. This difference suggests that the He I emission line originates from regions in the disc closer to the black hole than the regions responsible for the H α emission. The FWHM and velocity separation of the double peaks in the H α line (Table 1) are a factor 1.2–1.3 larger than the values reported during outburst (∼3300 km s^{-1} FWHM and $\Delta V^{pp} = 1790 \pm 67$ km s^{-1}; Corral-Santana et al. 2013). This difference is expected for a disc with a Keplerian velocity field since during outburst the disc increases its radius, thereby decreasing the velocity of the outer disc regions. The ∼138 Å FWZI of the H α and He I λ5876 implies projected velocities $\gtrsim$3150 and $\gtrsim$3520 km s^{-1} for the inner part of the accretion disc emitting at these wavelengths. The FWZI found for H α is a factor ∼1.6 larger than observed at different times during the outburst (Milisavljevic et al. 2011, see also fig. 1 in Corral-Santana et al. 2013). This difference in FWZI can be explained if the luminosity of the continuum decreased quicker than the luminosity of the emission lines when the source went from outburst to quiescence.

3.2 H α line profile time variability

We studied the variability of the H α line with diverse methods. These included single and two-Gaussian model fitting, the double-Gaussian technique described by Shafter, Szkody & Thorstensen (1986) and line EW measurements. The results obtained from these techniques are shown in Fig. 2. A single Gaussian fit to the line profiles yields radial velocities ranging from −189 to +118 km s^{-1}. These radial velocities reflect variations in the peak-to-peak intensities rather than changes in the line centroid (see below). The change in the double-peak intensity from almost symmetric peaks to enhanced redshifted or blueshifted peaks is obvious in Fig. 3 where we show the line profiles. Even though this behaviour could be naively attributable to an S-wave originating in a hotspot and/or the donor star, further inspection of the individual data in Fig. 3 shows that the presence of such a narrow component is not obvious. In addition, these variations in the profile structure can also not be explained as due to the eclipse of the accretion disc by the donor star. In such a scenario, the blueshifted disc emission is first eclipsed while the redshifted emission is eclipsed afterwards since the donor star initially occults disc regions moving towards the observer and subsequently blocks the receding regions from view. This is a distinctive rotational disturbance of the line profiles during eclipse, the so-called Z-wave. Thus, the changes in the H α line profile of J1357.2 do not show the Z-wave characteristic of emission line eclipses. The variations in the peak intensities are likely due to a highly variable non-uniform disc brightness distribution or/and departures from an axisymmetric flat disc. In this regard, we observe changes of up to 10 per cent in the peak-to-peak separation over successive spectra (see below). The short-term (suborbital) changes in the H α line profile morphology are reminiscent of those observed in the black hole low-mass X-ray binary (LMXB) GRO J0422+32 ($P_{orb} = 5.1$ h, $q = 0.12$) in quiescence (see fig. 1 in Filippenko, Matheson & Ho 1995). Another variable feature in the line shape is the depth of the central absorption delimited by the two line peaks. While the averaged line profile shows a moderately deep absorption, the individual spectra reveal that its depth can vary significantly during consecutive spectra. As observed in the first night (top-left panel, Fig. 3), the absorption core passes from being near the continuum level in the first spectrum to well above the continuum in the next one. Such deep cores are expected from discs observed at high inclination (see the Discussion).

Radial velocities were also derived with the double-Gaussian technique (Shafter et al. 1986) which consists of convolving the line profiles with two Gaussian bandpasses with separation a. After several trials, we chose to use a 200 km s^{-1} FWHM for both Gaussians. The separation a between the Gaussians was varied from 2300 to 6000 km s^{-1} in steps of 100 km s^{-1}. The radial velocity curves obtained with Gaussian separations $a \sim 2700$–3200 km s^{-1} displayed a modulation with a higher amplitude than found in the radial velocities determined with a one-Gaussian fit. We display in Fig. 2 the results for a Gaussian separation of 2800 km s^{-1}. At Gaussian separations larger than 3300 km s^{-1}, the radial velocities obtained with the double-Gaussian technique show no obvious modulation. Ideally the wings of disc emission lines should trace the motion of the compact object. In fact, by applying the above technique to their outburst data, Corral-Santana et al. (2013) recovered radial velocity modulations beyond $a = 3300$ km s^{-1} – note here that the H α line profile was narrower during outburst. In this way they were able to estimate the orbital period and the radial velocity semi-amplitude of the primary ($K_1 = 43 \pm 2$ km s^{-1}) for J1357.2. Our failure to do this could be primarily due to the systematic effects affecting the radial velocities (Section 2). The systematic velocity shifts could be comparable to or larger than K_1. Additionally, systematic effects are expected due to contamination of the red line wing by the overlapping He I λ6678 emission line.

The two-Gaussian model was employed to calculate both the peak-to-peak separation and the line centroid. The changes in the line morphology from near-symmetric to asymmetric double-peaked velocity profiles were taken into consideration when calculating these parameters. This was done because the Gaussian

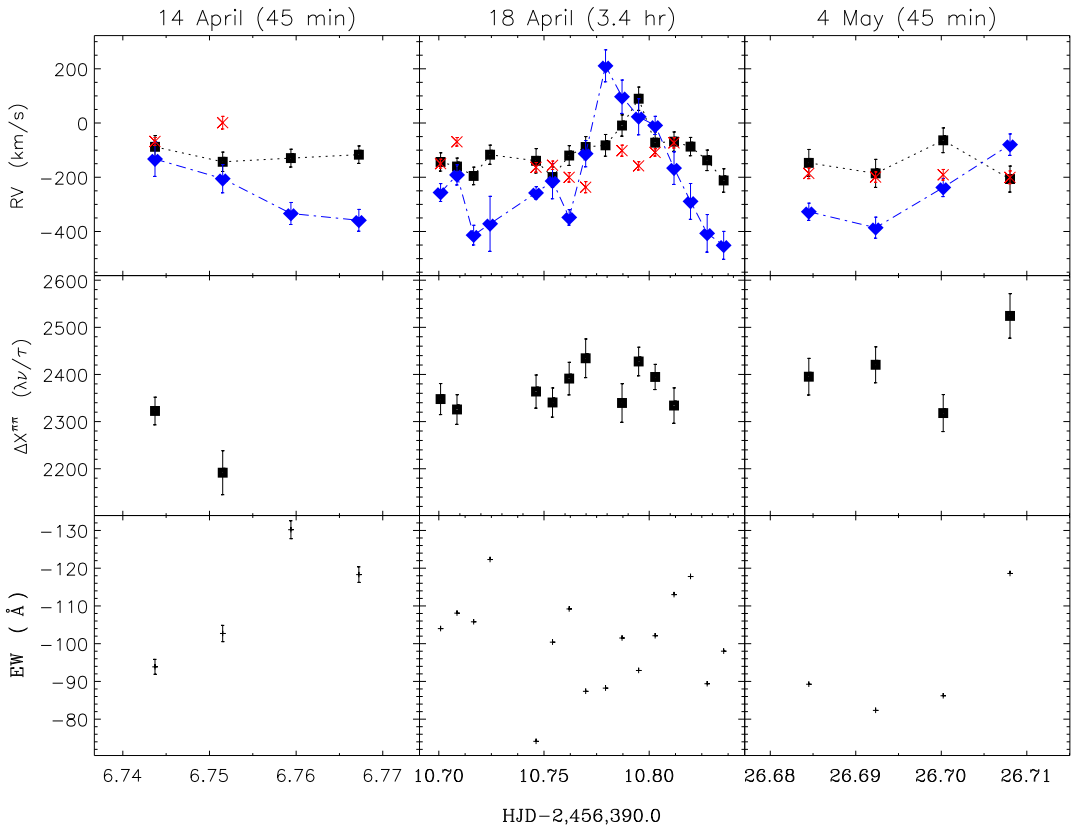

Figure 2. Hα emission line variability over the three nights of observations. Top: radial velocities from a single Gaussian fit (filled squares) and the double-Gaussian technique (filled diamonds). The line centroid derived with a two-Gaussian model is also shown (X). Middle: peak-to-peak separation (ΔV^{pp}) from the two-Gaussian model. Bottom: EW measured in the interval $\lambda\lambda$6460–6650.

component accounting for the weaker peak in the line will fit also part of the broader base of the profile. This yields a velocity that could be significantly offset from the real peak position in question. To avoid this possible bias effect, we examined each individual fit and rejected from our analysis V_b and V_r when either of the related Gaussian components had FWHM >45 km s^{-1}. This limit proved to be an effective quantitative way to select strongly (eight in total) asymmetric profiles – for comparison, the FWHMs of the two-Gaussians fit to the mean profile in Section 3.1 is ∼35 km s^{-1}. Note also that this non-physical two-component model yields reduced $\chi^2 = 1.0$ to 1.4, providing therefore statistically sound fits. By using profiles for which both Gaussian components have FWHM <45 km s^{-1} (16 spectra), we derive a mean peak-to-peak separation of $\overline{V_r - V_b} = 2370 \pm 70$ km s^{-1} and centroid of $(\overline{V_r + V_b})/2 = -130 \pm 60$ km s^{-1}. The uncertainties here and below correspond to the rms scatter. We also calculated the above line parameters by including velocity shifts obtained from the asymmetric profiles. For these profiles, only one of the two-Gaussian components in the fit is narrow (<45 km s^{-1} FWHM) yielding V_b (seven spectra) or V_r (one spectrum). Taking the mean of all the reliable velocity shifts ($\overline{V_b}$, $\overline{V_r}$), we derive $\overline{V_r} - \overline{V_b} = (1060 \pm 50) - (-1325 \pm 80) = 2390 \pm 100$ km s^{-1} and $\overline{V_r + V_b})/2 = -130 \pm 50$ km s^{-1}. The results from both calculations are fully consistent. The temporal variability for these two line parameters derived from the two-Gaussian model fitting is also displayed in Fig. 2 (top and middle panels). On April 18, the line centroid shows no clear modulation with velocities ranging from −222 to −50 km s^{-1}. The amplitude of the variations is lower than that obtained from velocities derived with the one-Gaussian model (300 km s^{-1} amplitude) and double-Gaussian technique (650 km s^{-1}). On May 4, the line centroid is constant during the 45-min length of the observations with a mean value of -180 ± 6 km s^{-1}. During the three nights, the peak-to-peak separation ranges from 2200 to 2530 km s^{-1}. Variations in the peak-to-peak separation can occur in short intervals as observed on April 14 and May 5 when in a ∼20-min interval changes of 130 ± 50 and 200 ± 60 km s^{-1} in amplitude take place. The fast changes (suborbital) in the peak-to-peak separation and intensities indicate that there are azimuthal variations in the outer disc velocities or structures.

The Hα EW varies irregularly as shown in the bottom of Fig. 2. With our 640 s integration, the EW ranges values from −73 to −129 Å with a mean of -100 ± 14 Å. The April 14 EW curve lacks any evidence for a decrease or increase in the line EW due to eclipses of the disc by the donor star. A decrease in the EW would occur at and near mid-eclipse if the disc regions responsible for the continuum and line are obscured from view by the donor star. On the other hand, an increase in EW can be associated with emission line regions in the disc that are not tightly confined to the orbital plane and thereby visible during eclipse. Examples of the increase in the Hα EW at eclipse time can be found in the neutron star LMXB sources X1822-371 ($P_{orb} = 5.1$ h; Harlaftis et al. 1997) and EXO 0748−676 ($P_{orb} = 3.8$ h; Pearson et al. 2006). None of these characteristics are present in the EW curve which appears dominated by erratic variations. For comparison with other black hole LMXBs in quiescence, the strength of Hα is not above than that found in GRO J0422+32 (−181 to −214 Å; Harlaftis et al. 1999).

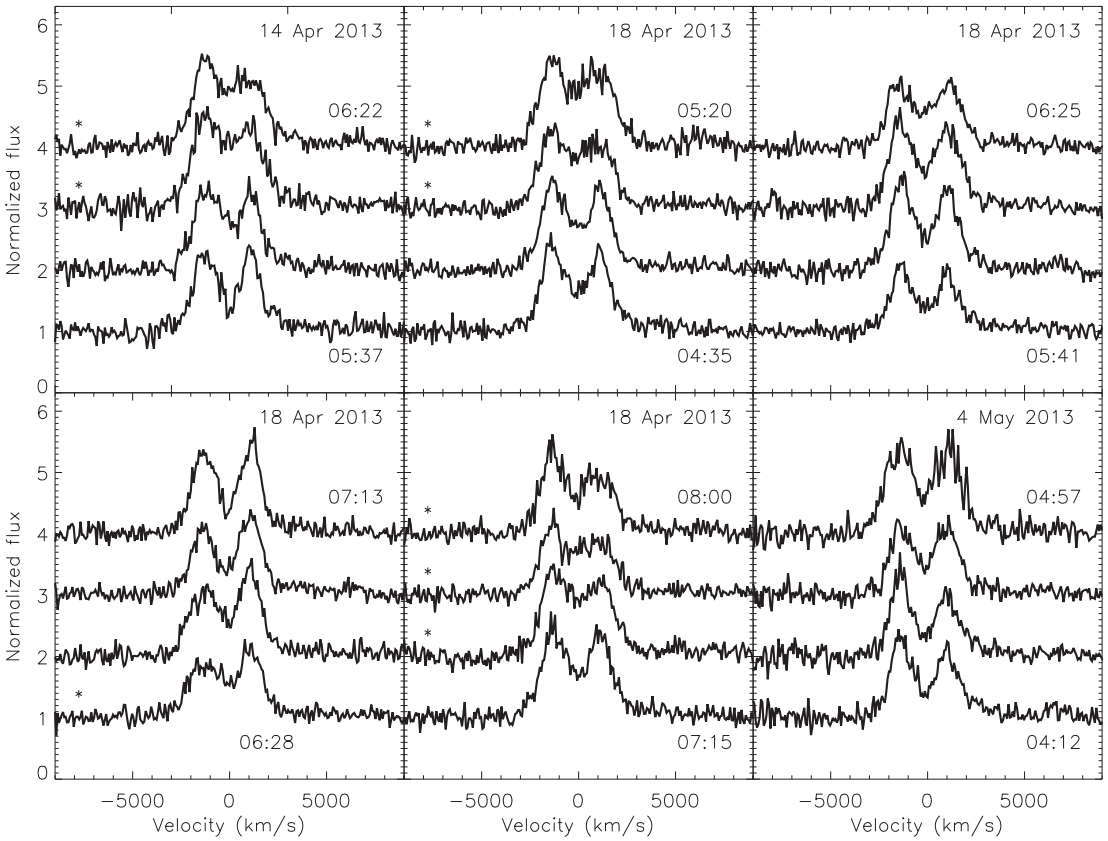

Figure 3. The 24 individual Hα line profiles covering different observing times. For the sake of clarity, each consecutive spectrum has been offset in the *Y*-direction. The starting and ending UT times of the spectroscopy obtained in the same OB are given in each panel. Note the changes in the depth of the absorption component in the line centre. An * marks the eight asymmetric profiles discussed in Section 3.2.

3.3 Further analysis: cross-correlation and Hα Doppler tomography

In order to search for signatures of the donor star that could have been cancelled out by averaging the data, we cross-correlated the individual spectra against SDSS (Abazajian et al. 2009) stellar templates covering spectral types between F and M. The cross-correlation was performed over sections free of telluric and emission line features. No cross-correlation functions were discernable from this analysis.

In an attempt to corroborate the 2.8-h orbital period, we performed Doppler tomography on the Hα line by phase folding the data over different trial periods and adopting a systemic radial velocity of $-150\,\mathrm{km\,s^{-1}}$ systemic (see Section 4.2). The tomograms (not shown) lead to variable asymmetries in the disc emission, but not to the extent that there was a clear favoured period. The reason why we were unable to use the tomographic reconstruction to constrain the orbital period is the lack of an S-wave that would have resulted in a strong emission feature in the tomogram.

4 DISCUSSION

Our optical spectroscopy of J1357.2 during quiescence shows no evidence for absorption features from the donor star. We therefore make use of the strong double-peaked Hα emission line to set constraints on the system parameters. For this, comparison will be drawn between the spectroscopic and photometric properties of J1357.2 and those observed in relevant types of accreting binaries such as accretion disc corona (ADC) systems and ultracompact binaries with a white dwarf accretor (better known as AM CVn systems). ADC sources are persistent LMXBs with an orbital inclination of $>80^{\circ}$. AM CVn systems have in common with short orbital period black hole LMXBs a low-mass ratio $q = M_2/M_1 \lesssim 0.1$, where M_2 and M_1 are the mass of the donor star and accreting object, respectively.

4.1 The radial velocity semi-amplitude of the donor star

Assuming an axisymmetric disc with gas in Keplerian motion, the projected motion of the outer edge of the disc $V_{\rm d}$ can be used to constrain the radial velocity semi-amplitude of the donor star (K_2) given that $K_2 < V_{\rm d}$. $V_{\rm d}$ has been determined for eight black hole LMXBs in quiescence by modelling the phase-averaged Hα line profile and by locating the hotspot in Doppler tomograms (e.g. Marsh, Robinson & Wood 1994; Orosz et al. 1994). In this way, it has been found that $V_{\rm d}({\rm H}\alpha)/K_2$ is between 1.11 and 1.47 (table 2 in Orosz et al. 2002). Using this empirical relationship and the Hα line observed in outburst, Corral-Santana et al. (2013) constrained $K_2 > 716 \pm 26\,\mathrm{km\,s^{-1}}$. For this they adopted $V_{\rm d}({\rm H}\alpha)/K_2 = 1.25$ (Orosz et al. 1994; Orosz & Bailyn 1995) and took into account that, since the source is in outburst, the peak-to-peak separation is less than $2 \times V_{\rm d}({\rm H}\alpha)$ during quiescence. Following a similar approach, we constrain K_2 to be $\gtrsim 796 \pm 7\,\mathrm{km\,s^{-1}}$ ($K_2 > 789\,\mathrm{km\,s^{-1}}$) by conservatively using $V_{\rm d}({\rm H}\alpha)/K_2 \leq 1.47$ during quiescence, the observational fact that $2 \times V_{\rm d}({\rm H}\alpha) \gtrsim \Delta V^{\rm pp}$ and $\Delta V^{\rm pp} = 2340 \pm 20\,\mathrm{km\,s^{-1}}$

as found from the averaged Hα profile during quiescence (Section 3.1). This implies a mass function $f(M_1) > 6.0\,M_\odot$ if J1357.2 is in a 2.8 ± 0.3 h orbit.

Adopting the radial velocity semi-amplitude of the primary ($K_1 = 43 \pm 2\,\mathrm{km\,s^{-1}}$; Corral-Santana et al. 2013) derived by applying the double-Gaussian technique to outburst data of the Hα emission line, a constraint for the mass ratio $q = K_1/K_2 \lesssim 0.054$ is obtained.

4.2 The systemic radial velocity

The characterization of the Hα profile performed in Section 3.2 shows that its centroid is offset to the blue on average by $130 \pm 50\,\mathrm{km\,s^{-1}}$. The position of a line originating in a disc will be shifted from its rest wavelength by the systemic radial velocity and primary's radial velocities at the time of the observation as: $\gamma + K_1 \sin 2\pi\phi$, where γ is the systemic radial velocity and ϕ is the orbital phase. Additional velocity components are usually present. They are due, for instance, to emission from the gas stream, hotspot and/or donor star. Furthermore, departures from a disc with gas in Keplerian motion are possible in LMXBs due to tidal effects on the disc. The tidal action of the donor on the outer parts of the disc can excite spiral shock patterns or cause the disc to elongate and precess. Disc precession can dominate the orbital-averaged velocity shifts observed in the emission line centroid. These contributions to the velocity profile can make it difficult to reliably establish γ or K_1 from time-resolved spectroscopy of emission lines (see e.g. Orosz et al. 1994 and section 7.5 in Shahbaz et al. 2013).

In what follows we present and discuss three pieces of observational evidence that indicate that the $-130\,\mathrm{km\,s^{-1}}$ offset of the Hα line centroid in J1357.2 most likely represents (within the errors) the systemic radial velocity: first, as reported in Section 3.2. the double-peaked Hα line profiles lack the presence of any narrow line component with velocity position modulated with the orbital motion. Therefore, J1357.2 shows no S-wave associated with emission from confined regions in the accretion flow (as discussed above) that can produce a radial velocity offset in an averaged line profile when the orbital phase coverage during the observations is non-uniform. S-waves are features commonly present in the time-resolved spectra of accreting binaries, but exceptions exist where this feature is not detected or is very weak. This is the case in GRO J0422+32 for which no S-wave was present in Hα spectroscopy during quiescence (Harlaftis et al. 1999). See also Mason et al. (2001) and Levitan et al. (2011) for examples of lack of/weak S-waves in a 1.8-h dwarf nova and in an AM CVn system, respectively. Secondly, the average radial velocity offset found during quiescence is fully consistent with the γ velocity of $\sim -150\,\mathrm{km\,s^{-1}}$ that can be derived from the diagnostic diagram for this Balmer line during outburst (fig. S2 in Corral-Santana et al. 2013). Thirdly, Corral-Santana et al. found γ and a periodic (likely orbital) modulation from spectroscopic data obtained in two outburst epochs separated by $\sim$20 d. The detection of an orbital modulation in the combined data sets is possible if any additional velocity shifts in the line centroid on a time-scale longer than the orbital period were small or if they had similar magnitude and sign at the time of the observations. For CVs and LMXBs with $q \lesssim 1/4$, long-term line shifts are expected during outburst due to disc eccentricity and precession. The formation of such a disc is attributed to the tidal influence of the donor star over a disc that during outburst radially expands to reaches the 3:1 resonance radius (see e.g. Hirose & Osaki 1990; Whitehurst & King 1991). The variations in the emission line centroids observed in XTE J1118+480 ($P_{\rm orb} = 4.08$ h, $q = 0.037$; Zurita et al. 2002; Torres et al. 2004) and AM Canum Venaticorum ($P_{\rm orb} = 17$ min, $q = 0.18$; Roelofs et al. 2006) provide evidence for the existence of large amplitude velocity shifts driven by a precessing disc. When present they can make it difficult to recover any orbital modulation superimposed on the lines by using data sets spanning many orbits and lacking enough orbital phase coverage at each epoch of observation. It appears therefore that long-term changes in the line centroid due to a precessing accretion disc were small or absent in J1357.2 (at least) at the time of the spectroscopic observations.

In support of the possibility of a non-precessing disc on J1357.2 is the absence of superhumps in the outburst light curves presented in Corral-Santana et al. (2013). Superhumps are photometric modulations that are driven by outbursts and characterized by having a periodicity a few per cent longer than the actual orbital period. This photometric behaviour is explained as due to the presence of the elliptical and precessing disc. Superhumps have been found during the outburst decline of the short orbital period black hole LMXBs GRO J0422+32 (O'Donoghue & Charles 1996), XTE J1118+480 (Uemura et al. 2000; Zurita et al. 2002, 2006) and Swift J1753.5−0127 ($P_{\rm orb} = 3.2$ h; Zurita et al. 2008). The apparent lack of superhumps in J1357.2 is striking, but not impossible given that these features do not necessarily develop or persist during all outbursts. A clear example is the eclipsing AM CVn system SDSS J0926+3624 ($P_{\rm orb} = 28$ min, $q = 0.04$) which exhibited superhumps in an outburst in 2006 and lacked these features in an outburst with similar brightness amplitude that occurred in 2009 (Copperwheat et al. 2011). Alternatively, the considerable dipping in the outburst light curve of J1357.2 might not have permitted the detection of the superhump signal which has been argued to be of low amplitude for high-inclination LMXBs (Haswell et al. 2001). However, see Mason et al. (2008) and Hakala et al. (2009) for the detection of superhumps in the ADC neutron star system MS 1603.6+2600 ($P_{\rm orb} = 1.9$ h).

In summary, the absence of S-wave components in the Hα line during quiescence, the similar values of the averaged line centroid during quiescence and the γ measured during outburst together with the apparent lack during outburst of significant long-term changes in the line strongly support the claim that the averaged centroid of the Hα line closely represents the systemic radial velocity of J1357.2. Since our radial velocities could have been affected to a greater or lesser degree by systematic effects (Section 2), we prefer and adopt for the rest of the discussion the value of $\gamma \sim -150\,\mathrm{km\,s^{-1}}$ derived in Corral-Santana et al. (2013).

4.3 The space velocity

Since the distance to J1357.2 is poorly constrained (0.5–6.3 kpc) and the proper motion is unknown, we cannot draw definitive conclusions on the space velocity of the source. Given the high Galactic latitude of J1357.2 ($b = 50^\circ$), the range of possible distances implies that the source lies between 0.4 and 4.8 kpc above the Galactic plane. With the known position and systemic radial velocity ($-150\,\mathrm{km\,s^{-1}}$), we can compute the Galactic space velocity components U, V and W for a grid of possible proper motions (in both right ascension and declination) and distances, using the transformations of Johnson & Soderblom (1987). We find that the W velocity component (motion perpendicular to the Galactic plane) is directed back towards the plane, unless the proper motions are large enough that the velocity components parallel to the plane of the disc deviate significantly (by $>150\,\mathrm{km\,s^{-1}}$) from the standard Galactic rotation at $240\,\mathrm{km\,s^{-1}}$ (Reid et al. 2014). This would imply that the source was originally at an even larger distance from the Galactic

plane. Either it is a halo object or (more likely) was formed in the disc and subsequently launched into an extremely elliptical orbit by a significant natal kick during the supernova explosion in which the black hole was formed, as also inferred to have occurred in GRO J1655−40 (Brandt, Podsiadlowski & Sigurdsson 1995) and XTE J1118+480 (Mirabel et al. 2001).

To place better constraints on the space velocity of J1357.2 would require knowledge of the source proper motion. However, since the quiescent counterpart of J1357.2 is fainter than *Gaia*'s limiting magnitude of $G = 20$, an accurate proper motion for J1357.2 would require VLBI observations, either of the (as-yet undetected) quiescent radio emission or of future transient outbursts (e.g. Mirabel et al. 2001; Russell et al. 2015).

4.4 The orbital inclination

An edge-on nature for J1357.2, as proposed to explain the profound dips in the optical light curves (Corral-Santana et al. 2013) is questionable. As argued by Armas-Padilla et al. (2014a), the X-ray spectrum during outburst shows an excess of soft emission attributable to non-occulted inner regions of the accretion disc. Moreover, the X-ray spectrum lacks emission/absorption X-ray features frequently observed in ADC sources (see section 4.1 in Armas-Padilla et al. 2014a) or in high-inclination neutron star LMXBs (Boirin et al. 2005; Díaz Trigo & Boirin 2013). Furthermore, there is another significant difference between J1357.2 in outburst and X-ray bright high-inclination systems (not necessarily ADC sources). In addition to extinction from interstellar matter, the $N_{\rm H}$ as measured in X-ray spectral fits usually includes the absorption associated with matter local to the source. The latter can be the dominant contribution to $N_{\rm H}$ when reddening towards the source is very low. In several high-inclination systems, the $N_{\rm H}$ determined from X-ray spectral fits is indeed dominated by extinction local to the source. For instance, ultraviolet observations have enabled reliable determinations of the interstellar reddening $E(B-V)$ towards EXO 0748−676 and X2127+119 (which have $P_{\rm orb} = 3.8$ and 17.1 h, respectively): for both sources $E(B-V) \sim 0.06$ mag (Ioannou et al. 2003; Pearson et al. 2006) equivalent to $N_{\rm H} \sim 3 \times 10^{20}$ cm^{-2} when using Bohlin, Savage & Drake (1978)'s $E(B-V)$ to $N_{\rm H}$ scaling. These values are much lower than $N_{\rm H}$ values found from X-ray fitting (see EXO 0748−676 Bonnet-Bidaud et al. 2001 and White & Angelini 2001 for X2127+119).

In other high-inclination sources, the $N_{\rm H}$ found for dipping and/or eclipsing LMXBs when using the out of dips or eclipse X-ray emission is typically of the order of 10^{21} cm^{-2} as found for MS 1603.6+2600 ($P_{\rm orb} = 1.9$ h; Hakala et al. 2005), XTE J1710−281 ($P_{\rm orb} = 3.8$ h (Younes, Boirin & Sabra 2009), X1822-371 ($P_{\rm orb} = 5.6$ h; Somero et al. 2012; Iaria et al. 2013), and other longer/shorter orbital-period high-inclination neutron star systems (Díaz Trigo et al. 2006).

Both the absolute value of $N_{\rm H}$ and the difference between the $N_{\rm H}$ from X-ray spectral fits and the optically derived equivalent $N_{\rm H}$ are very low for J1357.2. *Swift* data delivered $N_{\rm H}$ of $(1.2 \pm 0.7) \times 10^{20}$ cm^{-2} while fits to XMM data could not constrain it (Krimm et al. 2011b; Armas-Padilla et al. 2013). We can use the EWs of the interstellar Na doublet found in outburst (Torres et al. 2011) to estimate the interstellar reddening towards J1357.2. The resolved Na D1 and D2 components have ∼0.3 and ∼0.2 Å, respectively. We derive $E(B-V) \sim 0.1$ from the Na D1 line EW using the calibration of Munari & Zwitter (1997) and 0.05 from the Na D2 EW assuming a D2/D1 ratio of 2 (optically thin limit). Thus, $E(B-V)$ is likely 0.05–0.1 and thereby $N_{\rm H} = (3-6) \times 10^{20}$ cm^{-2} which is very similar to the $N_{\rm H}$ derived from the X-ray spectral fits given the systematic effects in both methods employed. On the basis of this, we conclude that J1357.2 has a low $N_{\rm H}$ when compared to the value expected from a dipping and/or eclipsing high-inclination LMXB. Possibly, the scaleheight of the material responsible for the local $N_{\rm H}$ enhancement is lower in J1357.2, or alternatively, the system inclination is lower than that of the high-inclination systems we compared with. But this seems to suggest that the inclination in J1357.2 is lower than what has been suggested previously and probably $\lesssim 80^\circ$. This would explain the lack of disc eclipses in the continuum or H$\,\alpha$ lines. Nevertheless, the orbital inclination of J1357.2 cannot be too low given the observed emission line characteristics. In particular, the depth of the absorption core defined by the line peaks is similar to that observed during quiescence in eclipsing CVs (Marsh, Horne & Shipman 1987) and is a strong indicator that the system has a high orbital inclination (Horne & Marsh 1986). We conclude that the inclination of J1357.2 is probably between 70–80°.

5 CONCLUSIONS

Optical spectra of J1357.2 during quiescence were analysed in this work. The average data show a continuum lacking photospheric lines from the donor star. Thus, we spectroscopically prove that synchrotron emission from a jet and/or thermal emission from the accretion disc fully veils the light contribution from the donor star at optical wavelengths. Broad strong H$\,\alpha$ and weaker He I emission lines are present in the data. The time-resolved H$\,\alpha$ line profile shows no strong S-wave patterns or other obvious periodic behaviour such as Z-wave caused by eclipses. We also find that no large long-term radial velocity shifts were present, either at the time of our spectroscopy or of the spectroscopy acquired in outburst. Thus, the data support a systemic velocity $\gamma = -150\,{\rm km\,s^{-1}}$ on the basis of the average radial velocity properties. From the H$\,\alpha$ peak-to-peak separation, we constrain K_2 to be $\gtrsim 796 \pm 7\,{\rm km\,s^{-1}}$ and $q \lesssim 0.054$. We estimate an interstellar absorption column towards the source of $(3-6) \times 10^{20}$ cm^{-2} which is comparable to that derived from X-ray fitting and lower than expected from an edge-on source. Therefore, the low X-ray brightness and spectral shape during outburst are unlikely due to a geometric effect (ADC system) and they are consistent with the source being in the low-hard state during the entire outburst. Although J1357.2 appears not to be one of the many missing eclipsing black hole LMXBs, the system has high inclination as inferred from the emission line morphology. Finally, we infer that the present Galactic kinematics of J1357.2 are such that its W space velocity component is directed towards the Galactic plane unless the proper motion is substantial.

ACKNOWLEDGEMENTS

We thank the anonymous referee for useful comments on the manuscript. We would like to thank Remco de Kok for an independent search for the cross-correlation signal from the donor star in J1357.2 and Jorge Casares for providing us with spectral templates used in these analysis. JCAMJ is the recipient of an Australian Research Council (ARC) Future Fellowship (FT140101082), and also acknowledges support from an ARC Discovery Grant (DP120102393). DS acknowledges support from STFC through an Advanced Fellowship (PP/D005914/1) as well as grant ST/I001719/1

REFERENCES

Abazajian K. N. et al., 2009, ApJS, 182, 543
Appenzeller I. et al., 1998, The Messenger, 94, 1
Armas-Padilla M., Degenaar N., Russell D. M., Wijnands R., 2013, MNRAS, 428, 3083
Armas-Padilla M., Wijnands R., Altamirano D., Méndez M., Miller J. M., Degenaar N., 2014a, MNRAS, 439, 3908
Armas-Padilla M., Wijnands R., Degenaar N., Muñoz-Darias T., Casares J., Fender R. P., 2014b, MNRAS, 444, 902
Bassa C. G., van Kerkwijk M. H., Koester D., Verbunt F., 2006, A&A, 456, 295
Bevington P. R., 1969, Data Reduction and Error Analysis for the Physical Sciences, McGraw-Hill, New York
Bohlin R. C., Savage B. D., Drake J. F., 1978, ApJ, 224, 132
Bonnet-Bidaud J. M., Haberl F., Ferrando P., Bennie P. J., Kendziorra E., 2001, A&A, 365, L282
Boirin L., Méndez M., Díaz Trigo M., Parmar A. N., Kaastra J. S., 2005, A&A, 436, 195
Brandt W. N., Podsiadlowski P., Sigurdsson S., 1995, MNRAS, 277, L35
Casares J., Torres M. A. P., Negueruela I., Gonzalez-Fernandez C., Corral-Santana J. M., Zurita C., Llano S. R, 2011, Astron. Telegram, 3206, 1
Copperwheat et al., 2011, MNRAS, 410, 1113
Corral-Santana J. M., Casares J., Muñoz-Darias T., Rodríguez-Gil P., Shahbaz T., Torres M. A. P., Zurita C., Tyndall A. A., 2013, Science, 339, 1048
Díaz Trigo M., Boirin L., 2013, Acta Polytech., 53, 659
Díaz Trigo M., Parmar A. N., Boirin L., Méndez M., Kaastra J. S., 2006, A&A, 445, 179
Filippenko A. V., Matheson T., Ho L. C., 1995, ApJ, 455, 614
Hakala P., Ramsay G., Muhli P., Charles P., Hannikainen D., Mukai K., Vilhu O., 2005, MNRAS, 356, 1133
Hakala P., Hjalmarsdotter L., Hannikainen D. C., Muhli P., 2009, MNRAS, 394, 892
Harlaftis E. T., Charles P. A., Horne K., 1997, MNRAS, 285, 673
Harlaftis E., Collier S., Horne K., Filippenko A. V., 1999, A&A, 341, 491
Haswell C. A., King A. R., Murray J. R., Charles P. A., 2001, MNRAS, 321, 475
Hirose M., Osaki Y., 1990, PASJ, 42, 135
Horne K., 1986, PASP, 98, 609
Horne K., Marsh T. R., 1986, MNRAS, 218, 761
Iaria R., Di Salvo T., D'Aì A., Burderi L., Mineo T., Riggio A., Papitto A., Robba N. R., 2013, A&A, 549, A33
Ioannou Z., van Zyl L., Naylor T., Charles P. A., Margon B., Koch-Miramond L., Ilovaisky S., 2003, A&A, 399, 211
Johnson D. R. H., Soderblom D. R., 1987, AJ, 93, 864
Krimm H. A. et al., 2011a, Astron. Telegram, 3138, 1
Krimm H. A., Kennea J. A., Holland S. T., 2011b, Astron. Telegram, 3142, 1
Levitan D. et al., 2011, ApJ, 739, 68
Marsh T. R., Horne K., Shipman H. L., 1987, MNRAS, 225, 551
Marsh T. R., Robinson E. L., Wood J. H., 1994, MNRAS, 266, 137
Mason E., Skidmore W., Howell S. B., Mennickent R. E., 2001, ApJ, 563, 351
Mason P. A., Robinson E. L., Gray C. L., Hynes R. I., 2008, ApJ, 685, 428
Milisavljevic D., Fesen R. A., Parrent J. T., Thorstensen J. R., 2011, Astron. Telegram, 3146, 1
Mirabel I. F., Dhawan V., Mignani R. P., Rodrigues I., Guglielmetti F., 2001, Nature, 413, 139
Munari U., Zwitter T., 1997, A&A, 318, 269
O'Donoghue D., Charles P. A., 1996, MNRAS, 282, 191
Orosz J. A., Bailyn C. D., 1995, ApJ, 446, L59
Orosz J. A., Bailyn C. D., Remillard R. A., McClintock J. E., Foltz C. B., 1994, ApJ, 436, 848
Orosz J. A. et al., 2002, ApJ, 568, 845
Pearson K. J. et al., 2006, ApJ, 648, 1169
Rau A., Greiner J., Filgas R., 2011, Astron. Telegram, 3140, 1
Reid et al., 2014, ApJ, 783, 130
Roelofs G. H. A., Groot P. J., Nelemans G., Marsh T. R., Steeghs D., 2006, MNRAS, 371, 1231
Russell T. D. et al., 2015, MNRAS, 450, 1745
Shafter A. W., Szkody P., Thorstensen J. R., 1986, ApJ, 308, 765
Shahbaz T., Russell D. M., Zurita C., Casares J., Corral-Santana J. M., Dhillon V. S., Marsh T. R., 2013, MNRAS, 434, 2696
Sivakoff G. R., Miller-Jones J. C. A., Krimm H. A., 2011, Astron. Telegram, 3147, 1
Somero A., Hakala P., Muhli P., Charles P., Vilhu O., 2012, A&A, 539, A111
Torres M. A. P., Callanan P. J., Garcia M. R., Zhao P., Laycock S., Kong A. K. H., 2004, ApJ, 612, 1026
Torres M. A. P., Steeghs D., Jonker P. G., Rauch M., 2011, Astron. Telegram, 3143, 1
Uemura M. et al., 2000, PASJ, 52, L15
White N. E., Angelini L., 2001, ApJ, 561, L101
Whitehurst R., King A., 1991, MNRAS, 249, 25
Younes G., Boirin L., Sabra B., 2009, A&A, 502, 905
Zurita C. et al., 2002, MNRAS, 333, 791
Zurita C. et al., 2006, ApJ, 644, 432
Zurita C., Durant M., Torres M. A. P., Shahbaz T., Casares J., Steeghs D., 2008, ApJ, 681, 1458

This paper has been typeset from a TEX/LATEX file prepared by the author.